

# A New Proposal to Jefferson Lab PAC48

## Measurement of the Two-Photon Exchange contribution to the electron-neutron elastic scattering cross section

S. Alsalmi (spokesperson)

*King Saud University, Riyadh 11451, Saudi Arabia*

E. Fuchey (spokesperson) and A.J.R. Puckett\*

*University of Connecticut, Storrs, Connecticut 06269, USA*

B. Wojtsekowski (spokesperson), S. Barcus\*, A. Camsonne\*, J-P. Chen\*,  
R. Ent\*, D. Gaskell\*, O. Hansen\*, M. Jones\*, C. Keppel\*, D. Mack\*,  
D. Meekins\*, R. Michaels\*, B. Sawatzky\*, G. Smith\*, and S. Wood\*

*Thomas Jefferson National Accelerator Facility, Newport News, Virginia 23606, USA*

J. Arrington\* and P. Reimer\*

*Argonne National Laboratory, 9700 S Cass Ave, Lemont, Illinois 60439, USA*

T. Averett\*

*The College of William and Mary, Williamsburg, Virginia 23185, USA*

K. Aniol\*

*California State University, Los Angeles, CA 90032, USA*

V. Bellini\*

*Istituto Nazionale di Fisica Nucleare, I-95123 Catania, Italy*

W. Boeglin\* and P. Markowitz\*

*Florida International University, Miami, FL 33199, USA*

G. Cates\*, K. Gnanvo\*, C. Gu\*, J. Liu\*, N. Liyanage\*,  
 V. Nelyubin\*, D. Nguyen\*, and C. Palatchi\*

*University of Virginia, Charlottesville, Virginia 232904, USA*

E. Cisbani\*, F. Meddi\*, and G. Urciuoli\*

*Istituto Nazionale di Fisica Nucleare - Sezione di Roma,*

*P.le Aldo Moro, 2 - 00185 Roma, Italy*

J.C. Cornejo\* and B. Quinn\*

*Carnegie Mellon University, Pittsburgh, Pennsylvania 15213, USA*

B. Crowe\* and B. Vlahovic\*

*North Carolina Central University, Durham, North Carolina 27707, USA*

D. Hamilton\* and R. Montgomery\*

*SUPA School of Physics and Astronomy,*

*University of Glasgow, Glasgow G12 8QQ, UK*

F. Hauenstein\*

*Old Dominion University, Norfolk, Virginia 23529, USA*

C. Petta\* and C. Suttera\*

*Istituto Nazionale di Fisica Nucleare, Dipt. di Fisica dell Univ. di Catania, I-95123 Catania, Italy*

G.G. Petratos\*

*Kent State University, Kent, OH 44242, USA*

A. Sarty\*

*Saint Mary's University, Halifax, Nova Scotia B3H 3C3, Canada*

K. Slifer\*

*University of New Hampshire, Durham, NH 03824, USA*

A. Shahinyan\*

*AANL, 2 Alikhanian Brothers Street, 0036, Yerevan, Armenia*

S. Širca\*

*Faculty of Mathematics and Physics, University of Ljubljana, 1000 Ljubljana, Slovenia*

E. Voutier\*

*Institut de Physique Nucléaire, 15 Rue Georges Clemenceau, 91400 Orsay, France*

(Dated: June 10, 2020)

## Abstract

We propose make a high precision measurement of the two-photon exchange contribution (TPE) in elastic electron-neutron scattering at a four-momentum transfer  $Q^2 = 4.5$   $(\text{GeV}/c)^2$ . While significant efforts to study the two-photon-exchange have focused around elastic electron-proton scattering, the impact of TPE on neutron form factors was never examined experimentally. The proposed experiment will provide the very first assessment of the two-photon exchange in electron-neutron scattering, which will be important for understanding of the nucleon form factor physics.

The proposed experiment will be performed in Hall A using the BigBite (BB) spectrometer to detect the scattered electrons and the Super-BigBite (SBS) to detect the protons and neutrons. The experiment should run concurrently with the E12-09-019  $G_M^n$  and E12-17-004  $G_E^n$ -Recoil experiments, which are expected to run in 2021. The experimental setup of the proposed experiment will be identical to that of E12-09-019 experiment.

The “ratio” method will be used to extract the electric form factor of the neutron  $G_E^n$  by scattering unpolarized electrons from deuterium quasi-elastically at two beam energies 4.4 and 6.6 GeV and electron scattering angles 41.9 and 23.3 degrees respectively. In the proposed approach, systematic errors are greatly reduced compared to those in the traditional single electron arm configuration. Several experiments at Mainz and JLab have used the ratio method to measure the neutron magnetic form factor in the past years. The method can be extended to extract the neutron electric form factor even with less stringent requirements on the knowledge of the absolute neutron detection efficiency and experimental kinematics.

## I. INTRODUCTION

In 1950's, a series of experiments performed by R. Hofstadter [1] revealed that the nucleons have a substructure (would be called later the quarks and gluons). The experiment confirmed M. Rosenbluth's theory [2] based on one-photon exchange approximation. In the Born approximation, where the interaction between the electron and the nucleon occurs *via* an exchange of a one virtual photon (OPE), the unpolarized  $e - N$  elastic cross section can be expressed in terms of a nucleon magnetic,  $G_M$ , and electric,  $G_E$ , form factors. These form factors describe the deviation from a point-like scattering cross section:

$$\left( \frac{d\sigma}{d\Omega} \right)_{eN \rightarrow eN} = \frac{\sigma_{Mott}}{\epsilon(1 + \tau)} [\tau \cdot G_M^2(Q^2) + \epsilon \cdot G_E^2(Q^2)] = \sigma_T + \epsilon \cdot \sigma_L, \quad (1)$$

where  $E$  and  $E'$  are the incident and scattered electron energies, respectively,  $\theta$  is the electron scattering angle,  $\tau \equiv -q^2/4M^2$ , with  $-q^2 \equiv Q^2 = 4EE' \sin(\theta/2)$  being the negative four momentum transfer square,  $M$  is the nucleon mass, and  $\epsilon = [1 + 2(1 + \tau) \tan^2(\theta/2)]^{-1}$  is the longitudinal polarization of the virtual photon,  $\sigma_L$  and  $\sigma_T$  are the cross sections for longitudinally and transversely polarized virtual photons, respectively.

14

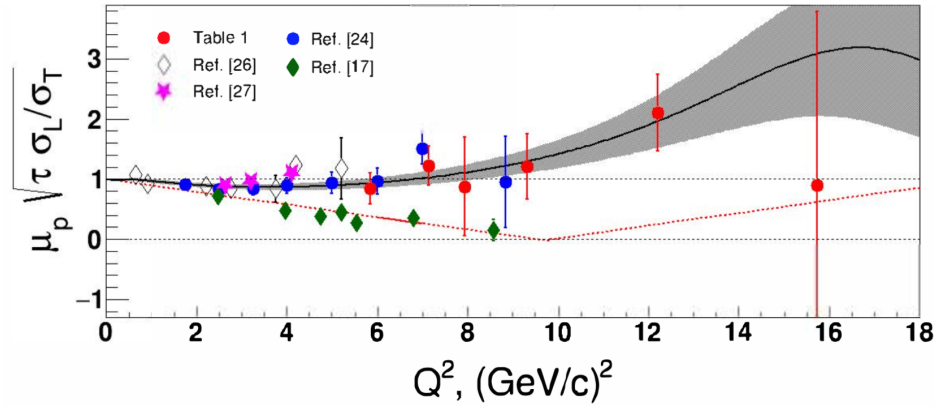


FIG. 1. The square root of Rosenbluth slope, corrected for kinematical factor  $\sqrt{\tau}$  and  $\mu_p$ , observed in elastic electron-proton scattering, adopted from Ref. [3].

The linear  $\epsilon$  dependence of the cross section is due to  $\sigma_L$  term, see Eq. 1. The ratio  $\sigma_L/\sigma_T$

is a Rosenbluth slope related to  $G_E/G_M$  (in OPE), see Fig. 1. The data show that at  $Q^2$  of 4-5  $(\text{GeV}/c)^2$  the Rosenbluth slope is three-four times larger than it suppose to be (in OPE) for the observed values of the  $G_E^p/G_M^p$  ratio.

The nucleon electromagnetic form factors can reveal a lot of information about the nucleon internal structure, as well as the quark distribution. The form factors depend only on one variable the negative square of the four-momentum transfer carried by the photon,  $Q^2$ . In the limit of large  $Q^2$ , pQCD provides well-motivated predictions for the  $Q^2$ -dependance of the form factors and their ratio. However, it was never predicted at what  $Q^2$  range the pQCD prediction (scaling) will be valid. Studies of GPDs show that pQCD validity will require a very large  $Q^2$  of 100  $(\text{GeV}/c)^2$ . It was discovered at JLab, using the double polarization methods, that the proton electric and magnetic form factors behave differently starting at  $Q^2 \approx 1 (\text{GeV}/c)^2$ .

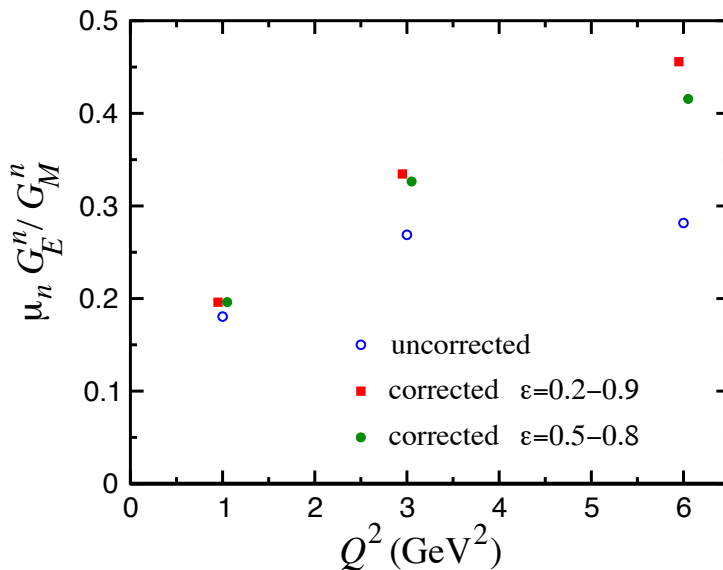


FIG. 2. Projected impact of TPE on  $G_E^n/G_M^n$  using LT separation, according to Ref. [4].

Experimentally, the nucleon form factors can be measured using one of two techniques: polarization transfer technique and Rosenbluth technique. The polarization method examines the polarization transfer from longitudinally polarized electron to the recoiling nucleon

and determine the resulting azimuthal asymmetry distribution using a polarimeter. Alternatively, one can use the polarized electron beam and a polarized target. While in the Rosenbluth method, the electric and magnetic form factors can be separated by making two or more measurements with different  $\epsilon$  values (*i.e.* different beam energies and angles), but with same  $Q^2$  value. Rosenbluth technique requires an accurate measurement of the cross section and suffers from large systematic uncertainties arising from several factors. For instance, an accurate knowledge of the neutron detector efficiency is required.

When comparing the values of  $G_E^p/G_M^p$  obtained from both techniques, a significant discrepancy was observed (see Fig. 1). Such discrepancy implies a potential problem in our understanding of the nucleon substructure. Many efforts were made in order to provide legitimate explanation, and it is believed that the inconsistency is due to contribution of two-photon exchange in  $e - N$  elastic scattering process, see Refs. [5, 6]. Predictions made for the neutron case are shown in Fig. 2, adopted from [4]. The contribution of TPE could reach about 30% of Rosenbluth slope value at 5 (GeV/c)<sup>2</sup>.

In the following we propose to make precision L/T separation of the elastic electron-neutron cross section and first experimental assessment of the two-photon exchange contribution on the neutron magnetic form factor measurements (see also Ref. [7]). The result of the nTPE experiment will likely add a new component to our understanding of the elastic electron-nucleon process.

50

## II. PHYSICS MOTIVATION

51       The nucleon plays the same central role in hadronic physics that the hydrogen atom does  
 52       in atomic physics and the deuteron in the physics of nuclei. The structure of the nucleon  
 53       and its general properties, such as (static) charge, magnetic moment, size, mass, and the  
 54       form factors and structure functions, are of fundamental scientific interest. The nucleon is a  
 55       laboratory for the study of the quark-gluon interaction and both nucleons, the proton and  
 56       the neutron, need to be explored. At present the proton has been more thoroughly studied  
 57       at large  $Q^2$  than the neutron. More data on the neutron is essential if we are to make real  
 58       progress in obtaining a complete description of the quark structure of the nucleon [8].

59       Considerable information on the structure of the nucleon has been obtained by using  
 60       electromagnetic probes via electron scattering. Inclusive deep inelastic scattering (DIS) has  
 61       been a classical tool with which the partonic structure of the nucleon has been probed. At  
 62       high  $Q^2$ , DIS yields information on the light-cone momentum space distributions of quarks  
 63       and gluons in the nucleon when viewed through the infinite momentum frame. Many of the  
 64       experimental foundations of QCD are in fact derived from investigations of various aspects  
 65       of DIS.

66       Exclusive processes, on the other hand, such as elastic electron and photon scattering,  
 67       can provide information on the spatial distribution of the nucleon's constituents, which is  
 68       parameterized through the elastic nucleon form factors. Experimental studies of elastic  
 69       electron scattering from both the proton and the neutron were initiated at SLAC and are  
 70       now being thoroughly performed at Jefferson Lab and other facilities world-wide.

71       The Dirac form factor,  $F_1$ , describes the distribution of the electric charge, while the  
 72       helicity non-conserving Pauli form factor,  $F_2$ , describes the distribution of the magnetic  
 73       moment; these two form factors are the ingredients of the hadronic current. These currents  
 74       contain information on the transverse charge distribution for an unpolarized and transversely  
 75       polarized nucleon, respectively, in the infinite momentum frame [9, 10].

76       The Sachs form factors,  $G_E$  and  $G_M$ , the ratio of which will be extracted directly from

<sup>77</sup> our data for the neutron, are related to  $F_1$  and  $F_2$  by

$$F_1 = \frac{G_E + \tau G_M}{1 + \tau} \text{ and } F_2 = \frac{G_M - G_E}{\kappa(1 + \tau)}, \quad (2)$$

<sup>78</sup> where  $\kappa$  is the nucleon anomalous magnetic moment.

<sup>79</sup> At asymptotically high  $Q^2$ , one can apply perturbative QCD (pQCD) to describe the  
<sup>80</sup>  $Q^2$  dependence of exclusive electron scattering. Early attempts to determine the scaling  
<sup>81</sup> behavior for  $F_1$  were performed by using a simple dimensional counting rule justified by the  
<sup>82</sup> inclusion of two gluon exchange processes [? ? ].

<sup>83</sup> A recent calculation by Belitski *et al.* [?] was performed where quark orbital angular  
<sup>84</sup> momentum was included to determine the behavior for the non-helicity conserving form  
<sup>85</sup> factor  $F_2$ . It was found to logarithmic accuracy that the ratio  $F_2/F_1$  should, at high  $Q^2$ ,  
<sup>86</sup> follow the form

$$\frac{F_2}{F_1} \propto \frac{\log^2(Q^2/\Lambda^2)}{Q^2}, \quad (3)$$

<sup>87</sup> This behavior was found to set in surprisingly early for the proton data for  $Q^2 > 2.0 \text{ GeV}^2$   
<sup>88</sup> with  $\Lambda \approx 300 \text{ MeV}$ . Using preliminary  $G_E^n$  data from E02-013 up to  $3.5 \text{ GeV}^2$ , this scaling  
<sup>89</sup> had not yet been observed [?] suggesting pQCD has not yet set in at this range in  $Q^2$ .  
<sup>90</sup> A calculation from ANL utilizing a Poincare invariant truncated Faddeev equation for a  
<sup>91</sup> quark-diquark system [?] suggests this type of behavior for each of the two nucleons may  
<sup>92</sup> be expected. For high  $Q^2$ , this experiment in conjunction with high  $Q^2 G_M^n$  data may be  
<sup>93</sup> able to observe the onset of this pQCD behavior in the neutron form factors.

<sup>94</sup> Over the years many QCD-inspired models have been developed to describe nucleon  
<sup>95</sup> electromagnetic form factors at small and intermediate  $Q^2$  values ( $Q^2 < 1-2 \text{ GeV}^2$ ). While  
<sup>96</sup> these have provided some insights into the possible origin of the nonperturbative quark  
<sup>97</sup> structure of the nucleon, ultimately one would like to use experimental form factor data to  
<sup>98</sup> test the workings of QCD itself.

<sup>99</sup> Recently, important developments in QCD phenomenology has been the exploration of  
<sup>100</sup> the generalized parton distribution (GPD) formalism [? ? ? ], which provides relations  
<sup>101</sup> between inclusive and exclusive observables. The nucleon elastic form factors  $F_1$  and  $F_2$  are

<sup>102</sup> given by the first moments of the GPDs

$$F_1(t) = \sum_q \int_0^1 H^q(x, \xi, t, \mu) dx \quad \text{and} \quad F_2(t) = \sum_q \int_0^1 E^q(x, \xi, t, \mu) dx, \quad (4)$$

<sup>103</sup> where  $H^q$  and  $E^q$  are two of the generalized parton distributions,  $x$  is the standard Bjorken  
<sup>104</sup>  $x$ ,  $\xi$  is the “skewness” of the reaction (Fig. ??),  $t$  is the four-momentum transferred  
<sup>105</sup> by the electron,  $\mu$  is a scale parameter necessary from the evolution over  $Q^2$ , analogous to  
<sup>106</sup> DIS parton distributions, and the sum is over all quarks and anti-quarks. These may be  
<sup>107</sup> accessed through processes such as deeply virtual compton scattering, where the interaction  
<sup>108</sup> is factorized into a hard part with the virtual photon/photon interactions with an individual  
<sup>109</sup> quark and a soft part of the residual system where the GPD information is contained, Fig. ??.

<sup>110</sup> Furthermore, as shown earlier by Ji [? ], the moments of GPDs can yield information,  
<sup>111</sup> according to the Angular Momentum Sum Rule, on the contribution to the nucleon spin  
<sup>112</sup> from quarks and gluons, including both the quark spin and orbital angular momentum.

<sup>113</sup> At present, experimental measurements of GPDs are scarce. Until such data becomes  
<sup>114</sup> available, work has been done to attempt to parameterize these GPDs, which rely heavily on  
<sup>115</sup> data from electromagnetic form factors and parton distributions from DIS as constraints [?  
<sup>116</sup> ? ? ]. Data at high  $Q^2$  for  $G_E^n$  would contribute significantly in the development of these  
<sup>117</sup> models.

<sup>118</sup> The isovector and isoscalar form factors constructed from the proton and neutron form  
<sup>119</sup> factors have different sensitivity to higher Fock components of the light cone quark wave  
<sup>120</sup> function. This difference can be an important handle to test the valence quark dominance in  
<sup>121</sup> exclusive reactions in the few  $(\text{GeV}/c)^2$  range. Data on  $F_{1p}$  and  $F_{1n}$  will allow the extraction  
<sup>122</sup> of information related to the  $(u-d)$  distribution, which was calculated recently using the GPD  
<sup>123</sup> approach by K. Goeke, M. Polyakov, and M. Vanderhaeghen [? ].

<sup>124</sup> Recent theoretical developments also indicate that measurements of the individual elastic  
<sup>125</sup> form factors of the nucleon up to high  $Q^2$  may shed light on the problem of nucleon spin [?  
<sup>126</sup> ].

<sup>127</sup> As an incidental benefit of the proposed experiment, a better determination of the neutron  
<sup>128</sup> electric form factor will be very important for calculations of nuclear form factors, such as

<sub>129</sub> those of the deuteron. Even though  $G_E^n \ll G_E^p$  at  $Q^2 \approx 0$ , at larger  $Q^2$  ( $Q^2 \sim 3 \text{ GeV}^2$ ) the ratio  
<sub>130</sub>  $G_E^n/G_E^p$  can be as large as  $\approx 0.4$ , so that accurate information on  $G_E^n$  at large  $Q^2$  is essential  
<sub>131</sub> for a reliable description of the deuteron form factors.

132

### III. TECHNIQUE

133 The neutron form factors are challenging to be determine experimentally especially be-  
 134 cause there is no free neutron target. However, since the deuterium is a loosely coupled  
 135 system, it can be viewed as the sum of a proton target and a neutron target. In fact, quasi-  
 136 elastic scattering from deuterium has been used to extract the neutron magnetic form factor,  
 137  $G_M^n$ , at modestly high  $Q^2$  for decades [11, 12] in the single arm ( $e, e'$ ) experiments. How-  
 138 ever, the proton cross section needs to be subtracted by applying a single-arm quasi-elastic  
 139 electron-proton scattering. This “proton-subtraction” technique suffers from a number sys-  
 140 tematic uncertainties e.g. contributions from inelastic and secondary scattering processes.

141 Many year ago, L. Durand [13] proposed the so-called “ratio-method” based on the mea-  
 142 surement of both  $D(e, e'n)$  and  $D(e, e'p)$  reactions. In this method, many of the systematic  
 143 errors are cancel out. Several experiments [14–16] have applied the ratio-method to determine  
 144 the neutron magnetic form factor. We propose to use this method to measure Rosenbluth  
 145 slope and extract (in OPE approximation) the neutron electric form factor,  $G_E^n$ .

146 Data will be collected for quasi-elastic electron scattering from deuteron in process  
 147  $D(e, e'n)p$ . A complementary  $D(e, e'p)n$  data will be taken to calibrate the experiment ap-  
 148 paratus. The current knowledge of the  $e - p$  elastic scattering cross section (obtained in the  
 149 single arm  $H(e, e')p$  and  $H(e, p)e'$  experiments) will be also used for precision determination  
 150 the experiment kinematics.

151 Applying Rosenbluth technique to measure  $G_E^n$  requires accurate measurement of the cross  
 152 section and suffers from large uncertainties. To overcome this issue, we propose to extract  
 153 the value of  $G_E^n$  from the measured the ratio of quasi-elastic yields,  $R_{n/p}$ , in scattering from  
 154 a deuteron target as follows:

$$R_{n/p} \equiv R_{observed} = \frac{N_{e, e'n}}{N_{e, e'p}} \quad (5)$$

155  $R_{observed}$  needs to be corrected to extract the ratio of e-n/e-p scattering from nucleons:

$$R_{corrected} = f_{corr} \times R_{observed} , \quad (6)$$

156 where the correction factor  $f_{correction}$  takes into account the variation in the hadron efficiencies  
 157 due to changes of  $e - N$  Jacobian, the radiative corrections, and absorption in path from the  
 158 target to the detector, and small re-scattering correction.

159 In one-photon approximation,  $R_{corrected}$  can be presented as:

$$R_{corrected} = \frac{\sigma_{Mott}^n \cdot (1 + \tau_p)}{\sigma_{Mott}^p \cdot (1 + \tau_n)} \times \frac{\epsilon \sigma_L^n + \sigma_T^n}{\epsilon \sigma_L^p + \sigma_T^p} \quad (7)$$

It is important that the ratio  $R_{Mott} = \frac{\sigma_{Mott}^n \cdot (1 + \tau_p)}{\sigma_{Mott}^p \cdot (1 + \tau_n)}$  could be determined with very high relative accuracy even with modest precision for the beam energy, electron scattering angle, and detector solid angle. Now, let us write the  $R_{corrected}$  at two values of  $\epsilon$  using  $R_c^{n(p)} = \sigma_L^{n(p)} / \sigma_T^{n(p)}$  as:

$$R_{corrected,\epsilon_1} = R_{Mott,\epsilon_1} \times \frac{\epsilon_1 \sigma_L^n + \sigma_T^n}{\epsilon_1 \sigma_L^p + \sigma_T^p} \quad R_{corrected,\epsilon_2} = R_{Mott,\epsilon_2} \times \frac{\epsilon_2 \sigma_L^n + \sigma_T^n}{\epsilon_2 \sigma_L^p + \sigma_T^p}$$

In these two equations there are two unknown variables:  $\sigma_L^n$  and  $\sigma_T^n$ . The dominant contribution to the uncertainty of the slope of the cross section vs.  $\epsilon$ ,  $S_c^n = \sigma_L^n / \sigma_T^n$ , will come from the uncertainty of  $S_c^p$ . At  $Q^2=4.5$  (GeV/c)<sup>2</sup>, according to the global analysis of  $e - p$  cross section [3], the value of  $S_c^p$  is close to  $1/(\tau \mu_p^2) = 0.107$  with uncertainty of 0.01. The resulting equation for  $S_c^n$  is:

$$A = B \times \frac{1 + \epsilon_1 S_c^n}{1 + \epsilon_2 S_c^n} \approx B \times (1 + \Delta \epsilon \cdot S_c^n),$$

160 where the variable  $A = R_{corrected,\epsilon_1} / R_{corrected,\epsilon_2}$  will be measured with relative precision of  
 161 0.1%. Assuming, for this estimate, equal values of  $Q^2$  for two kinematics, the  $\tau$  and  $\sigma_T$  for  
 162 two kinematics are canceled out, and the variable  $B = R_{Mott,\epsilon_1} / R_{Mott,\epsilon_2} \times (1 + \epsilon_2 S_c^p) / (1 + \epsilon_1 S_c^p)$ .  
 163 For actual small range of  $\epsilon$  and small value of the slope, the  $B \approx (1 - \Delta \epsilon \cdot S_c^p)$ . The value  
 164 of  $B$  will be determined from global proton  $e - p$  data to a precision of  $0.25 \times 0.01$ .

165 At  $Q^2=4.5$  (GeV/c)<sup>2</sup> the ratio  $\mu_n G_E^n / G_M^n$  is of  $0.55 \pm 0.05$ , see the review [17]. In a  
 166 simplest model, the slope  $S_c^n$  is a sum of the slope due to  $G_E^n / G_M^n$  and the TPE contribution.  
 167 If we use for TPE the prediction [4], shown in Fig. 2, the TPE leads to increase of  $S_c^n$  by a  
 168 factor of 2, so the result of this experiment for TPE will be  $0.069 \pm 0.012 \pm 0.01$ , where the  
 169 first uncertainty is due to accuracy of  $G_E^n / G_M^n$  and the second one due to projected precision  
 170 of this experiment. It would be a 4-4.5 sigma observation of the neutron TPE.

171

#### IV. EXPERIMENTAL SETUP

172 As illustrated in Fig. 3, this experiment will study electron scattering from a 15 cm  
 173 long liquid Deuterium target held in a vacuum. The scattered electron will be detected  
 174 in the BigBite spectrometer with an upgraded electron detector stack. The neutron arm is  
 175 arranged with a dipole magnet 48D48 (SBS) and a segmented hadron calorimeter HCAL. The  
 176 whole detector package was designed and is now under assembling for the GMn, E12-09-019,  
 177 experiment.

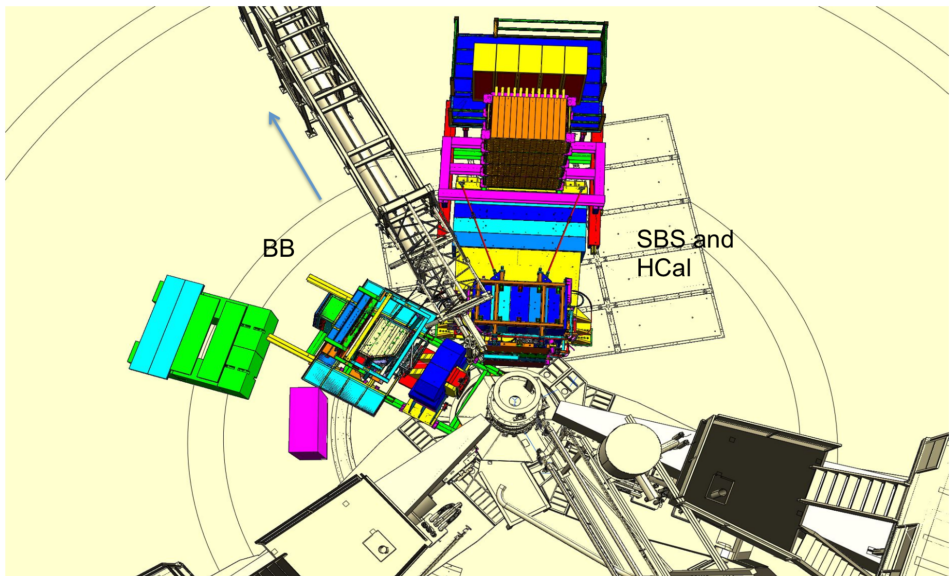


FIG. 3. Layout of the experimental setup in nTPE.

178

##### 1. Parameters of the SBS

179 The 48D48 magnet from Brookhaven was acquired as part of the Super Bigbite project  
 180 and will be available for this experiment. It consists of a large dipole magnet which provides  
 181 a field integral of about  $1.7 \text{ T} \cdot \text{m}$ , allowing for quasielastic protons to be sufficiently deflected  
 182 to allow clear differentiation from neutrons. The active field volume has an opening of  $46 \times$   
 183  $25 \text{ vertical} \times \text{horizontal}$ ), matching the aspect ratio of the neutron arm, and a depth of 48  
 184 cm.

185      The placement of this magnet will be 1.6 m away from the target, which would normally  
186      interfere with the beamline. To accommodate this, modifications were made to the iron yoke  
187      such that the beamline will pass through the magnet yoke area.

188      The field configuration will be such that positively charged particles will be deflected  
189      upwards away from the hall floor. For a field integral of 1.7 Tesla-m, protons of momentum  
190      2.5 GeV/c will be deflected 250 mrad, which translates to a displacement of xxm. Including  
191      expected detector resolution, the  $p_{miss,\perp}$  distribution will be similar to what was seen in  
192      E02-013, so cuts of < 100 MeV/c will be appropriate. Monte Carlo simulations show a  
193      contamination of charged quasielastics to be negligible.

194      The presence of the magnet also works to sweep low energy charged particles from the  
195      target away from the neutron arm. Particles of momentum less than 1.3 GeV/c will be  
196      entirely swept outside of the neutron arm acceptance. This greatly reduces the amount of  
197      charged low energy background.

198

### A. The BigBite Spectrometer

199 Scattered electrons will be detected in the BigBite spectrometer. The spectrometer con-  
 200 sists of a single dipole magnet (with magnetic field approximately 1.2 Tesla-m and a detection  
 201 system, see Fig. 4.

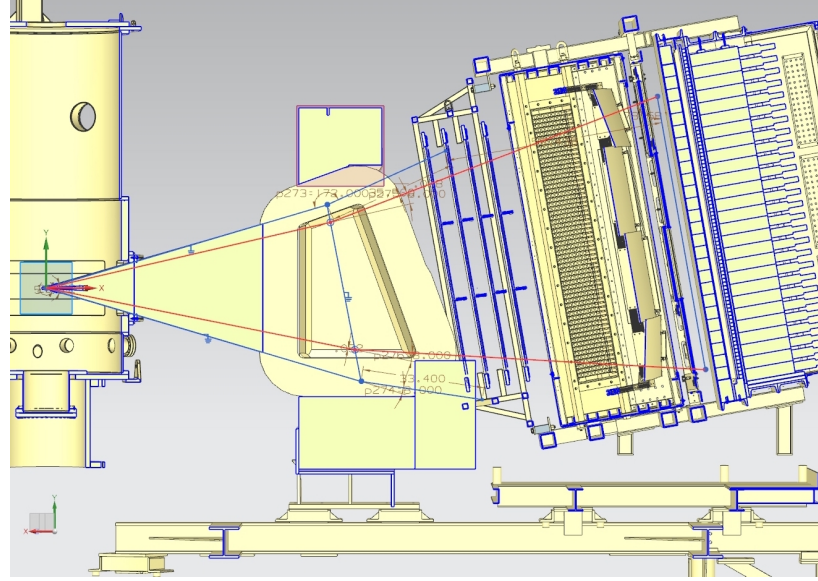


FIG. 4. The BigBite spectrometer with the upgraded detector stack.

202

#### 1. Simulation of BigBite

203

#### 2. Detector Package

- 204    a. Background Rate in BigBite
- 205    b. Front GEM chambers
- 206    c. Gas Cherenkov Counter
- 207    d. Rear GEM chamber
- 208    e. Shower and Preshower
- 209    f. Timing Scintillator Hodoscope

210

### 3. Trigger

211

#### 4. Simulation of BigBite

212

a. Rates in the detectors

213

b. Trigger rate and efficiency

214

**B. Neutron Detector**

215 S

216

*1. Structure of the Neutron Detector*

217       **V. SIMULATIONS, ESTIMATIONS OF COUNTING RATES AND**  
 218       **ACCIDENTALS**

219       The estimations of counting rates accidentals have been performed using G4SBS, the  
 220       GEANT4-based simulation package developed for the SBS experiment [? ]. This package  
 221       includes a wide range of event generators, which allows to evaluate the rates for both events  
 222       of interest (signal) and background. The representation of the experiment apparatus in  
 223       G4SBS is shown in the high  $\epsilon$  configuration on Fig. 5.

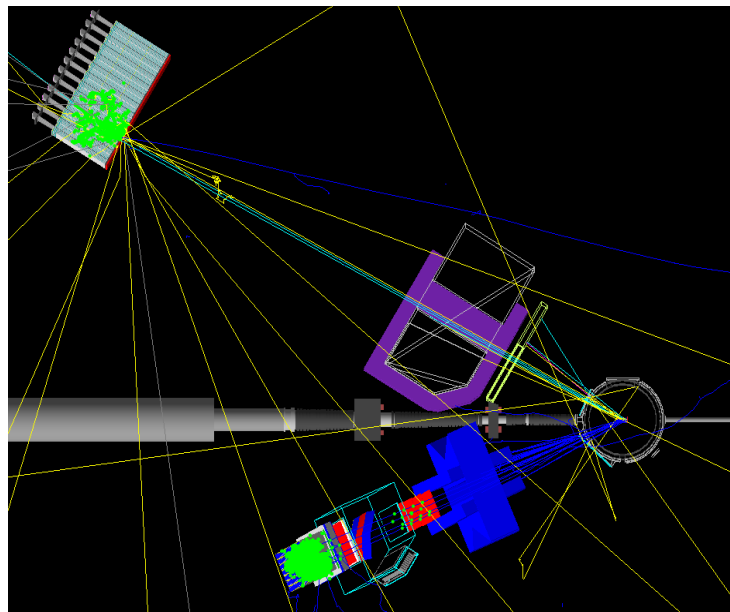


FIG. 5. Top view of the experimental apparatus model in G4SBS, shown in the high  $\epsilon$  configuration. The beam direction is indicated, as well as the main elements (HCAL, SBS magnet, BigBite spectrometer)

224  
 225       **A. Background and trigger rates**

227       The main processes expected to contribute the trigger rates for the BigBite spectrometer  
 228       are:

229 • the inelastic electron nucleon scattering process;

230 • photons from inclusive  $\pi^0$  production;

231 • and to a lesser extent, charged pions.

232 One the other hand, we expect all sorts of hadronic backgrounds to contribute to the rates in  
 233 HCal, the dominant ones being pions. Both the inelastic scattering and the inclusive neutral  
 234 and charged pion production are implemented in G4SBS, the latter relying on the Wiser  
 235 parametrization [? ]. We may also considered the minimum-bias “beam-on-target” gener-  
 236 ator for the HCal background, especially at lower angle (all electromagnetic and hadronic  
 237 processes being built-in in G4SBS).

238 The thresholds to apply to each arm are determined as a function of the elastic peak. For  
 239 the electron arm, the threshold has been set at  $\mu_E - 2.5\sigma_E$ ,  $\mu_E$  and  $\sigma_E$  being respectively  
 240 the position and width of the fitted elastic peak. Fig. 6 presents the distributions of rate of  
 241 energy deposit for the different processes involved in the BigBite trigger rates.

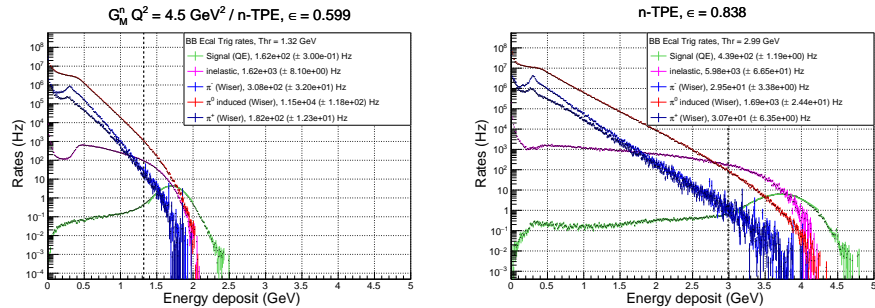


FIG. 6. Rates of the different process contributing to the BigBite electron arm trigger, for the low  $\epsilon$  (left) and the high  $\epsilon$  (right). Quasi-elastic is in green, inelastic in magenta,  $\pi^0$  in red,  $\pi^-$  in blue, and  $\pi^+$  in dark blue. Note the resolution for the elastic peak in the BigBite shower is  $\sim 0.3$  GeV.

242

243

244 Since HCal is a sampling calorimeter (meaning that only a fraction of the shower energy  
 245 is measured), it's resolution is significantly wider ( $\sim 0.7$  GeV). Due to this, the threshold  
 246 is at 90% efficiency (which corresponds to  $\sim 0.1$  GeV for both kinematics. Fig. 7 presents

247 the distributions of rate of energy deposit for the different processes involved in the BigBite  
 248 trigger rates.

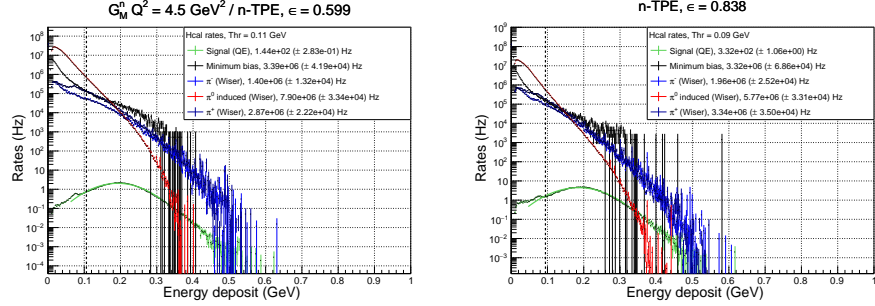


FIG. 7. Rates of the different process contributing to the HCal trigger, for the low  $\epsilon$  (left) and the high  $\epsilon$  (right). Quasi-elastic is in green, minimum bias in black,  $\pi^0$  in red,  $\pi^-$  in blue, and  $\pi^+$  in dark blue. Note the peak itself is around 0.2 GeV for 3.2 GeV nucleons.

249

250

251 The thresholds and trigger rates for each arm, as well as the coincidence rate (assuming  
 252 30ns coincidence window), are summarized in Table. I.

253

254 Note that for HCal, the “total rates” is either the sum of inclusive charged and neutral pions  
 255 evaluated with the Wiser cross sections *or* the “minimum bias” beam on target. We have  
 256 good reasons to think that the Wiser code results actually overestimate the HCal rates, but  
 257 for the sake of thoroughness, we have checked the coincidence rates assuming the sum of the  
 258 inclusive pions (evaluated with the Wiser cross sections) as the HCal rates.

259 In the worst case scenario, the coincidence rates could be as high as 5kHz, which might be  
 260 at the limit of manageability for the DAQ. However, a slight increase on the HCal threshold  
 261 (which would drop the efficiency from  $\sim 90\%$  to  $\sim 85\%$ ) would decrease the total HCal rates by  
 262  $\sim 35\%$  to 40% in this worst case scenario, which would make the situation more manageable  
 263 (3.3 kHz).

Point ( $\epsilon$ )	1 (0.599)		2 (0.838)	
	BigBite rates (Hz)	HCal rates (Hz)	BigBite rates (Hz)	HCal rates (Hz)
threshold (GeV)	1.32	0.106	2.99	0.090
Quasi-elastic	$1.62 \times 10^2$	$1.44 \times 10^2$	$4.39 \times 10^2$	$3.48 \times 10^2$
Inelastic	$1.62 \times 10^3$	-	$5.98 \times 10^3$	-
$\pi^-$ (Wiser)	$3.08 \times 10^2$	$1.40 \times 10^6$	$2.95 \times 10^2$	$1.96 \times 10^6$
$\pi^0$ (Wiser)	$1.15 \times 10^4$	$7.90 \times 10^6$	$1.69 \times 10^3$	$5.77 \times 10^6$
$\pi^+$ (Wiser)	$1.82 \times 10^2$	$2.87 \times 10^6$	$3.07 \times 10^2$	$3.34 \times 10^6$
Minimum bias	-	$3.39 \times 10^6$	-	$3.32 \times 10^6$ (*)
<i>Total</i>	$1.37 \times 10^4$	$1.22 \times 10^7$	$8.17 \times 10^3$	$1.11 \times 10^7$
(min. bias - HCal only)		/ $3.39 \times 10^6$		/ $3.32 \times 10^6$
<b>Coincidence rate</b>	$5.01 \times 10^3$		$2.72 \times 10^3$	
(with min. bias HCal)	$1.39 \times 10^3$		$8.14 \times 10^2$	

TABLE I. Trigger rates for BigBite and HCal, with the different process contributions separated, and the sum. For HCal, the total rates is either the sum of the (Wiser) inclusive pions or the minimum bias. The coincidence rates assume a 30 ns coincidence window.

264

## B. Accidentals: contamination from inelastic

265

The main source of contamination for the quasi-elastic comes from the inelastic electron-nucleon scattering. Most of this contamination can be cleaned out thanks to a selection on the center of mass energy

$$W^2 = M_N^2 + 2M_N^2(E - E') - Q^2, \quad (8)$$

268 and the missing transverse momentum of the nucleon

$$p_{\perp miss} = \sqrt{(q_x - p'_x)^2 + (q_y - p'_y)^2}, \quad (9)$$

269 where  $M_N$  is the mass of the nucleon,  $E$  and  $E'$  the initial and final energy of the electron,  
270 and  $q_{x,y}$ ,  $p'_{x,y}$  are the projections on  $x$ ,  $y$  of the vectors of the virtual photon and final nucleon.

271 The distributions of these quantities (weighted with cross section and including detector res-  
 272 olutions) are displayed for quasi-elastic and inelastic scattering, and for proton and nucleon,  
 273 on Fig. 8 for the low  $\epsilon$  kinematic, and on Fig. 9 for the high  $\epsilon$  kinematic. Provided that

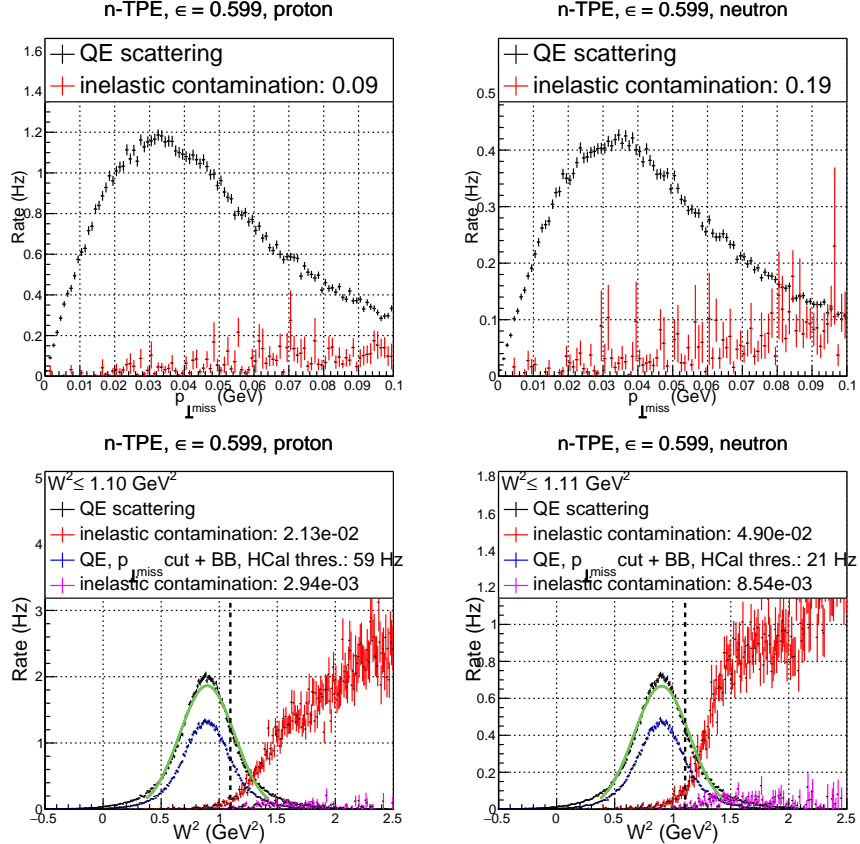


FIG. 8. Compared quasi-elastic and inelastic distributions (including detectors resolutions) for  $p_{\perp miss}$  (top) and  $W^2$  (bottom), for the low  $\epsilon$  kinematic. Comparison for protons is on the left, and comparison for neutrons is on the right. On the bottom panel, black and red are before the  $p_{\perp miss} \leq 0.1$  GeV selection, while blue and magenta are after  $p_{\perp miss} \leq 0.1$  GeV selection and application of BigBite shower and HCal thresholds.

274

276

277 we are not limited by statistics and the sample purity is capital for our experiment, we set  
 278 the selection criteria on  $W^2$  and  $p_{\perp miss}$  to maximize inelastic contamination (ideally below  
 279 1 %). Setting  $p_{\perp miss} \leq 0.1$  GeV and  $W^2 \leq 1.1$  GeV $^2$ , the inelastic contamination of the

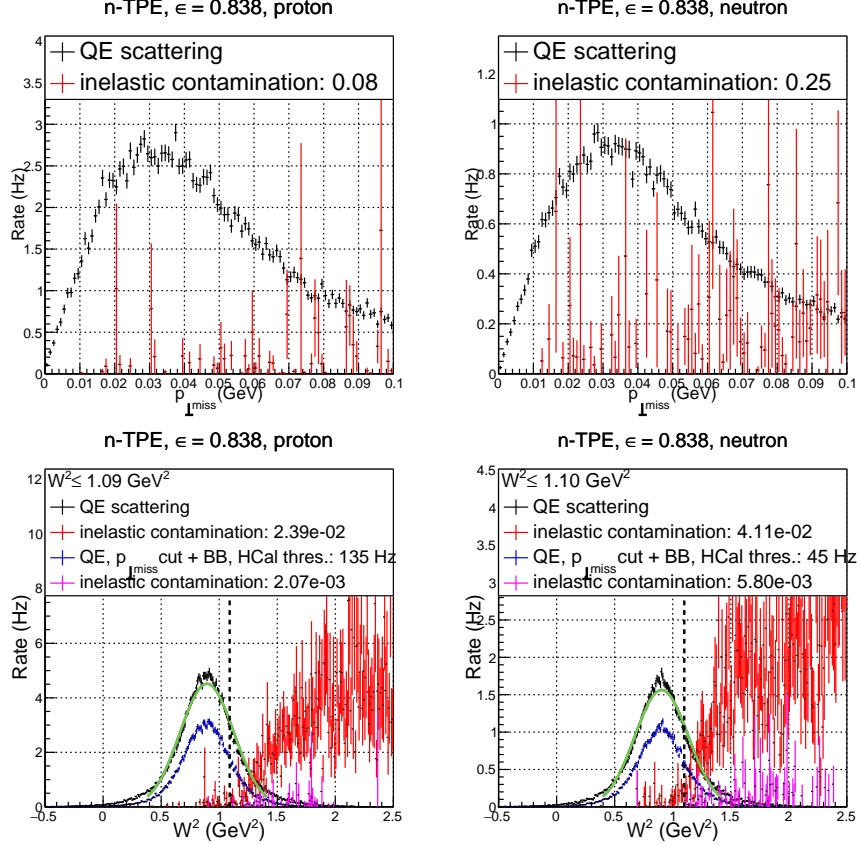


FIG. 9. Compared quasi-elastic and inelastic distributions (including detectors resolutions) for  $p_{\perp \text{miss}}$  (top) and  $W^2$  (bottom), for the high  $\epsilon$  kinematic. Comparison for protons is on the left, and comparison for neutrons is on the right. On the bottom panel, black and red are before the  $p_{\perp \text{miss}} \leq 0.1$  GeV selection, while blue and magenta are after  $p_{\perp \text{miss}} \leq 0.1$  GeV selection and application of BigBite shower and HCal thresholds.

<sup>280</sup> elastic sample ranges from 0.2 % to 0.9 %, while retaining  $\geq 60$  %.

281

### C. Quasi-elastic counting rates

<sup>282</sup> The signals for this experiment have been generated using the G4SBS elastic/quasi-elastic  
<sup>283</sup> generator. We generated 1M events sample for each kinematics, on a solid angle that was  
<sup>284</sup> larger than the detector acceptance. To evaluate the detector solid angle, we define simple

<sup>285</sup> criteria that each event has to pass, defined as the following;

- <sup>286</sup> • require a primary track, going through all 5 GEM layers (electron arm);
- <sup>287</sup> • require non-zero energy deposit in both the preshower and shower (electron arm);
- <sup>288</sup> • require non-zero energy deposit in HCal (hadron arm).

<sup>289</sup> The detector solid angle, for both proton and neutron, are defined in Table. II

Point ( $\epsilon$ )	$\Delta\Omega_e$ (msr)	$\Delta\Omega_e \otimes \Delta\Omega_n$ (msr)	$\Delta\Omega_e \otimes \Delta\Omega_p$ (msr)
1 (0.599)	52.4	46.7	47.2
2 (0.838)	32.7	20.8	22.2

TABLE II. Kinematics electron solid angle, and convoluted electron/hadron solid angle

<sup>290</sup>

<sup>291</sup> Then, we evaluate the detection efficiency. For the electron, we require the energy recon-  
<sup>292</sup> structed in the BigBite calorimeter to be above a threshold defined as  $thr = \mu_E - 2.5 * \sigma_E$ ,  
<sup>293</sup> as well as a minimum number of GRINCH PMTs fired due to the primary electron; For  
<sup>294</sup> HCal, we require the threshold to be such as we obtain 90% efficiency. These values are  
<sup>295</sup> summarized in Table. III.

Point ( $\epsilon$ )	BB thr. (GeV)	HCal thr. (GeV)	$\eta_{det,e}$	$\eta_{det,n}$	$\eta_{det,p}$	$\eta_{QEsel,n}$	$\eta_{QEsel,p}$
1 (0.599)	1.32	0.11	0.902	0.904	0.892	0.589	0.605
2 (0.838)	2.99	0.09	0.808	0.889	0.882	0.617	0.647

TABLE III. Kinematics electron thresholds, particle detection efficiencies ( $\eta_{det}$ ), and efficiency of  
quasi-elastic selection  $\eta_{QEsel}$  separated for the proton and the neutron.

<sup>296</sup>

297 The counting rates are evaluated using the events that have passed the selection described  
 298 above, and weighting those events with the cross section calculated by G4SBS, multiplied  
 299 by the generation solid angle, using the formula:

$$N_{est} = \mathcal{L}\Delta t \times \sum_{i \in \text{accepted evts}} \frac{d\sigma}{d\Omega} * \Delta\Omega_{Gen}/N_{Gen} \quad (10)$$

300 Events are “accepted” if they meet the following criteria:

- 301 • the electron is in the BigBite acceptance;
- 302 • the electron passes the BigBite threshold defined in Table III and gives signal in the  
 303 GRINCH;
- 304 • the nucleon is in the HCal acceptance and passes the HCal threshold defined in Ta-  
 305 ble III;
- 306 • the event passes the quasi-elastic selection defined in the previous section *i.e.*  $W^2 \leq 1.1 \text{ GeV}^2$   
 307 and  $p_{\perp miss} \leq 0.10 \text{ GeV}$ .

308 The counting rates, as well as the reduced cross section  $F^2$  and its error  $\Delta F^2 = F^2/\sqrt{N_{QE}}$   
 309 are compiled for both kinematics in Table. IV, assuming a running time  $\Delta t = 12$  hours of  
 310 running at a beam intensity of  $I_{exp} = 30 \mu\text{A}$  on a liquid deuterium target with length  
 311  $l_{tgt} = 15 \text{ cm}$  and density  $d_{tgt} = 0.169 \text{ g.cm}^{-3}$ .

Point ( $\epsilon$ )	QE $e-n$ counts	QE $e-p$ counts	$F_n^2$ ( $\times 10^{-3}$ )	$\Delta F_n^2$ ( $\times 10^{-6}$ )	$F_p^2$ ( $\times 10^{-3}$ )	$\Delta F_p^2$ ( $\times 10^{-6}$ )
1 (0.599)	$9.07 \times 10^5$	$2.55 \times 10^6$	0.99	1.04	2.73	1.70
2 (0.838)	$1.94 \times 10^6$	$5.83 \times 10^6$	0.72	0.52	1.93	0.80

TABLE IV. Quasi-elastic counting rates, and “reduced cross section” as defined by Eq. ???. These rates assume  $\Delta t = 12$  hours of running at a beam intensity of  $I_{exp} = 30 \mu\text{A}$  on a liquid deuterium target with length  $l_{tgt} = 15 \text{ cm}$  and density  $d_{tgt} = 0.169 \text{ g.cm}^{-3}$

<sup>313</sup> The expression of  $F_2$  is:

$$F^2 = \frac{N_{QE}}{\mathcal{L}_{exp} \cdot \Delta t \cdot d\sigma_{Mott}/d\Omega \cdot \Delta\Omega \cdot \eta} \quad (11)$$

<sup>314</sup> where  $\Delta t$  the running time,  $\Delta\Omega$  is the convoluted BigBite-HCal solid angle,  $\eta$  is the product  
<sup>315</sup> of all efficiencies (detection efficiencies  $\eta_{det} \times$  selection efficiency  $\eta_{QEsel}$ ) , and  $\mathcal{L}_{\text{luminosity}}$  is the  
<sup>316</sup> experimental luminosity:

$$\mathcal{L}_{exp} = \frac{I_{exp}}{q_e} * L_{tgt} * d_{tgt} \frac{\mathcal{N}_A}{m_D}. \quad (12)$$

<sup>317</sup> The calculation of the  $F_2$  term requires the evaluation of the Mott cross section

$$\frac{d\sigma_{Mott}}{d\Omega} = (\hbar c \alpha_{EM})^2 \left( \frac{1}{2E} \right)^2 \left( \frac{\cos\theta_e/2}{\sin^2\theta_e/2} \right)^2 \frac{E'}{E} \quad (13)$$

<sup>318</sup> The Mott cross section has been calculated with the weighted average of the electron variables  
<sup>319</sup> (momentum and polar angle).

Point ( $\epsilon$ )	$\langle \theta_e \rangle$	$\langle k' \rangle$	$\langle Q^2 \rangle$	$\sigma_{Mott}$
	(deg)	(GeV)	(GeV $^2$ )	(nb sr $^{-1}$ )
1 (0.599)	41.7	2.01	4.47	6.62
2 (0.838)	22.9	4.26	4.40	48.0

TABLE V. Cross-section weighted average of kinematic variables over the BigBite acceptance. The Mott cross section has been evaluated at these values.

<sup>320</sup>

321

## VI. PROPOSED MEASUREMENTS

322 We propose to use the same experimental setup of E12-09-019 experiment. We will add  
 323 a kinematic point at  $Q^2 = 4.5 \text{ (GeV/c)}^2$ , but with a higher  $\epsilon$  value. This additional point  
 324 along with the data point of E12-09-019 experiment will allow us to perform LT separation  
 325 and obtain (in one-photon approximation) the  $G_E^n$  value. Table 1 displays the kinematic  
 326 setting of the proposed experiment.

Point	$Q^2$ (GeV/c) <sup>2</sup>	E (GeV)	E' (GeV)	$\theta_{BB}$ degrees	$\theta_{SBS}$ degrees	$\epsilon$ (%)	$\Delta\sigma$ (%)	$\Delta TPE$ (%)
1	4.5	4.4	2.0	41.88	24.67	0.599		
2	4.5	6.6	4.2	23.23	31.2	0.838		

TABLE VI. Kinematic settings of the proposed experiment. The blue row is a kinematic point of E12-09-019 experiment.

327

328

## VII. BEAM TIME REQUEST

329     **We request 48 hours total time (32 hours of beam-on target)** to measure the  
 330 two-photon effect (and  $G_E^n$  in one-photon approximation) at  $Q^2 = 4.5$  (GeV/c)<sup>2</sup> through a  
 331 measurement of the cross sections of the reaction D(e,e'N) at a large value of the virtual  
 332 photon polarization  $\epsilon=0.84$ . This experiment will take place in Hall A, utilizing the Big-  
 333 Bite spectrometer to detect electrons scattered off the liquid deuterium target, and HCal  
 334 calorimeter to detect the recoiling neutron and proton.

335     Data taking (if approved by PAC48) will take place in summer 2021 during the approved  
 336 and scheduled run of the GMn, E12-09-019, experiment, which is going to measure the  $e - n$   
 337 elastic scattering cross section at  $Q^2 = 4.5$  (GeV/c)<sup>2</sup> at  $\epsilon=0.60$ .

338     The set of instrumentation and required beam current for proposed measurement is iden-  
 339 tical to one in the GMn experiment. The beam energy of 6.6 GeV will be used. One of two  
 340 data points required for the cross section LT separation is already in the data taking plan of  
 341 GMn.

342     There are no other measurements of TPE in the  $e - n$  elastic scattering and knowledge  
 343 of the TPE is essential for the understanding of the elastic electron scattering from neutron  
 344 (and proton) and hadron structure. Furthermore, it is a necessary input in the analysis and  
 345 interpretation of a wide range of electron scattering processes.

346     The kinematics of our measurements emphasize the same  $Q^2$  range where TPE in  $e - p$   
 347 elastic scattering was observed to dominate in Rosenbluth slope. Measuring at this high  
 348 momentum transfers will provide unique input for testing TPE calculations [4].

349     We propose to measure the Rosenbluth slope and extract (in one-photon approximation)  
 350  $\delta G_E^n / G_M^n$  to an accuracy of 0.15, which would bring its precision to a level comparable with  
 351 that of the double polarization experiments GEN-RP and GEN-He3 at such value of  $Q^2$ .  
 352 Such precision should be sufficient to detect the TPE contribution to the  $e - n$  Rosenbluth  
 353 slope on the three sigma level.

- 
- 354 [1] R. Hofstadter, *Rev. Mod. Phys.* **28**, 214 (1956).
- 355 [2] M. N. Rosenbluth, *Phys. Rev.* **79**, 615 (1950).
- 356 [3] E. Christy *et al.*, “Two-photon exchange in electron-proton elastic scattering at large four-momentum transfer,” (2020), in preparation for publication in PRL.
- 357
- 358 [4] P. G. Blunden, W. Melnitchouk, and J. A. Tjon, *Phys. Rev.* **C72**, 034612 (2005), arXiv:nucl-th/0506039 [nucl-th].
- 359
- 360 [5] J. Arrington, P. G. Blunden, and W. Melnitchouk, *Prog. Part. Nucl. Phys.* **66**, 782 (2011), arXiv:1105.0951 [nucl-th].
- 361
- 362 [6] A. Afanasev, P. Blunden, D. Hasell, and B. Raue, *Prog. Part. Nucl. Phys.* **95**, 245 (2017), arXiv:1703.03874 [nucl-ex].
- 363
- 364 [7] B. Wojtsekhowski, in *Exclusive processes at high momentum transfer. Proceedings, Newport News, USA, May 15-18, 2002* (2002) arXiv:1706.02747 [physics.ins-det].
- 365
- 366 [8] G. D. Cates, C. W. de Jager, S. Riordan, and B. Wojtsekhowski, *Phys. Rev. Lett.* **106**, 252003 (2011), arXiv:1103.1808 [nucl-ex].
- 367
- 368 [9] G. A. Miller, *Phys. Rev. Lett.* **99**, 112001 (2007), arXiv:0705.2409 [nucl-th].
- 369 [10] C. E. Carlson and M. Vanderhaeghen, *Phys. Rev. Lett.* **100**, 032004 (2008), arXiv:0710.0835 [hep-ph].
- 370
- 371 [11] E. B. Hughes, T. A. Griffy, M. R. Yearian, and R. Hofstadter, *Phys. Rev.* **139**, B458 (1965).
- 372 [12] R. G. Arnold *et al.*, *Phys. Rev. Lett.* **61**, 806 (1988).
- 373 [13] L. Durand, *Phys. Rev.* **115**, 1020 (1959).
- 374 [14] E. E. W. Bruins *et al.*, *Phys. Rev. Lett.* **75**, 21 (1995).
- 375 [15] G. Kubon *et al.*, *Phys. Lett.* **B524**, 26 (2002), arXiv:nucl-ex/0107016 [nucl-ex].
- 376 [16] J. Lachniet *et al.* (CLAS), *Phys. Rev. Lett.* **102**, 192001 (2009), arXiv:0811.1716 [nucl-ex].
- 377 [17] V. Punjabi, C. F. Perdrisat, M. K. Jones, E. J. Brash, and C. E. Carlson, *Eur. Phys. J.* **A51**, 79 (2015), arXiv:1503.01452 [nucl-ex].
- 378